Supporting Information for

Performing homogeneous catalytic ozonation using heterogeneous Mn^{2+}-bonded oxidized carbon nanotube by self-driven pH variation induced reversible desorption and adsorption of Mn^{2+}

Jing Wang,[†] Xie Quan,[†] Shuo Chen,[†] Hongtao Yu,[†] and Yongsheng Chen[‡]*

[†]Key Laboratory of Industrial Ecology and Environmental Engineering (Ministry of Education), School of Environmental Science and Technology, Dalian University of Technology, Dalian 116024, China

[‡]School of Civil and Environmental Engineering, Georgia Institute of Technology, Atlanta, Georgia 30332, United States

* Corresponding author. Tel: +86-411-84706140.

E-mail address: quanxie@dlut.edu.cn

This supplementary material is a 19-page document, which consists of 7 tables, 24 figures, experimental section, references and this cover page.

Experimental Section

Chemicals and Materials

Pristine CNTs (multiwalled, length: 15 μm, outer diameter: 10-20 nm) was acquired from Shenzhen Nanotech Port Co., Ltd., China. 5-tert-Butoxycarbonyl-5-methyl-1-pyrroline-N-oxide (BMPO) was provided by the Dojindo China Co., Ltd. (Shanghai, China). 2,2,6,6-tetramethyl-4-piperidinol (TEMP) was purchased from the Shanghai Aladdin Biochemical Technology Co., Ltd. (Shanghai, China). Other chemicals and reagents used in all experiments were of analytical grade and purchased from the Damao chemical Reagent Factory (Tianjin, China). Ultrapure water (resistivity >18 MΩ cm) was obtained from an OKP ultrapure water system and was used in all experiments.

GC-MS Analysis

To allow gas chromatography-mass spectrometry (GC-MS) measurement of non-water, the first step of detecting organic acid intermediates was to esterify and extract samples by the procedure described by Li et al.[1] Typically, 6 mL sample were esterified in a 40-mL sealed bottle at 75 ^{o}C for 40 min by adding 4 mL of n-butanol (HPLC grade) and 4 mL of concentrated HCl (37%). After cooling, 12 mL of hexane (HPLC grade) was added into the mixed solution with violent shaking to extract the esterified products. The extraction was repeated twice. The extracted liquid was dewatered by anhydrous sodium sulfate and concentrated to 200 μL by nitrogen purging. Finally, the obtained samples were analyzed by GC-MS. The Agilent 6890N GC (Agilent Technologies, Santa Clara, CA, USA) equipped with an Agilent DB-5MS capillary column (30 m × 0.250 mm × 0.25 μm) followed by an Agilent 5975 MS detector. The initial column temperature began at 50 ^{o}C and ramped at 20 ^{o}C min^{-1} to 280 ^{o}C with a holding time of 2 min for each increment. For detecting aromatic intermediates, the samples were extracted by the mixture of n-hexane and dichloromethane ($V_{n\text{-hexane}}$: $V_{dichloromethane}$ = 1:1). The initial column temperature began at 60 ^{o}C and ramped at 10 ^{o}C min^{-1} to 80 ^{o}C, then ramped at 4 ^{o}C min^{-1} to 100 ^{o}C, and finally ramped at 10 ^{o}C min^{-1} to 300 ^{o}C with a holding time of 10 min.

The Quantification of Organic Acid Intermediates

Maleic Acid detected by HPLC. An HPLC equipped with a UV detector (Photodiode Array Detector 2996) and a SunFire C18 column (5 μm × 4.6 mm × 250 mm, Waters) was used to detect the concentration of maleic acid. The mobile phase was KH_2PO_4-H_3PO_4 buffer solution (0.01 mM)/methanol at a volume ratio of 97/3, at a temperature of 35 ^oC. The flow rate was set at 0.7 mL min^{-1} (λ = 220 nm).

Oxalic Acid detected by HPLC. The mobile phase was $NH_4H_2PO_4$ solution (2 wt‰)/methanol at a volume ratio of 98/2. The temperature was 25 ^oC, and the flow rate was set at 0.7 mL min^{-1} (λ = 197 nm).

Acetic Acid and Formic Acid detected by IC. An IC equipped with a ThermoScientific® Dionex IonPac AG23 Guard column (4 × 50 mm) was used to detect the concentrations of acetic acid and formic acid. The mobile phase was 4.5 mM Na_2CO_3/0.8 mM $NaHCO_3$.

EPR experiments

BMPO-•OH spin adducts: Center field: 3385.0 G; Sweep Width: 100 G; Modulation Frequency: 100 kHz; Modulation Amplitude: 1.00 G; sweep time, 40.96 s; microwave frequency, 9.528 GHz; microwave power, 21.43 mW.

BMPO-$O_2^{\bullet-}$ spin adducts: Center field: 3360.0 G; Sweep Width: 200 G; Modulation Frequency: 100 kHz; Modulation Amplitude: 2.00 G; sweep time, 327.68 s; microwave frequency, 9.445 GHz; microwave power, 16.26 mW.

TEMP-$^1O_2$ spin adducts: Center field: 3360.0 G; Sweep Width: 100 G; Modulation Frequency: 100 kHz; Modulation Amplitude: 2.00 G; sweep time, 245.76 s; microwave frequency, 9.446 GHz; microwave power, 2.80 mW.

Batch Desorption Experiment

The effect of pH on the adsorption of dissolved Mn^{2+} on OCNT surfaces was carried out in a 0.2 L beaker at room temperature. The concentration of Mn^{2+}-OCNT was controlled to be the same as the Mn^{2+}-OCNT/O_3 system. The pH of suspension was first adjusted to 3.5 by 0.1 M HCl solution. The adsorption experiments of dissolved Mn^{2+} on OCNT surfaces were examined after the desorption equilibrium. Briefly, the Mn^{2+}-OCNT suspension was dispersed by ultrasonic dispersion, then the pH of

suspension was first adjusted to 3.5 and kept stirring for 30 min. Five milliliters of the suspension was sampled and filtrated through a 0.22 μm acetate fiber filters at predetermined time intervals. Then the adsorption experiments were carried out under different pH values. The pH of the suspension was adjusted by 0.1 M NaOH solution. The suspension was kept shaken for 10 min under each pH value, and was sampled to test the Mn^{2+} concentration in solution.

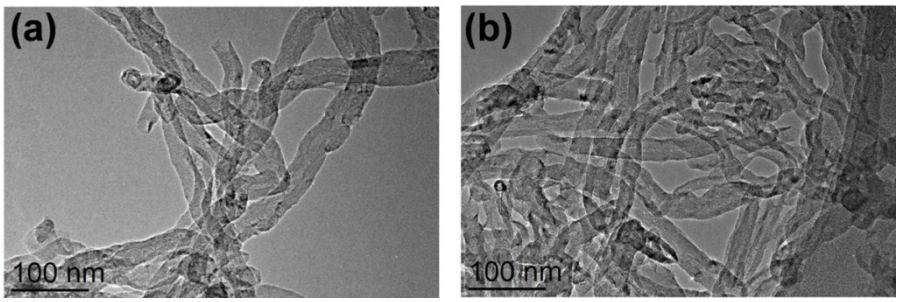

Fig. S1 TEM image of (a) pristine CNT and (b) CNT-80°C

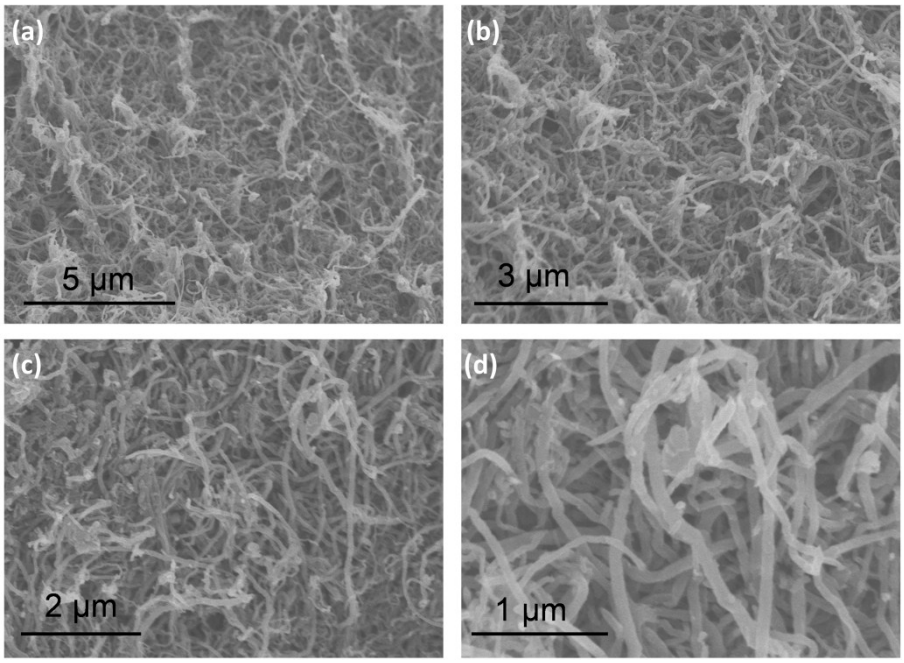

Fig. S2 SEM images of Mn^{2+}-OCNT with different sizes.

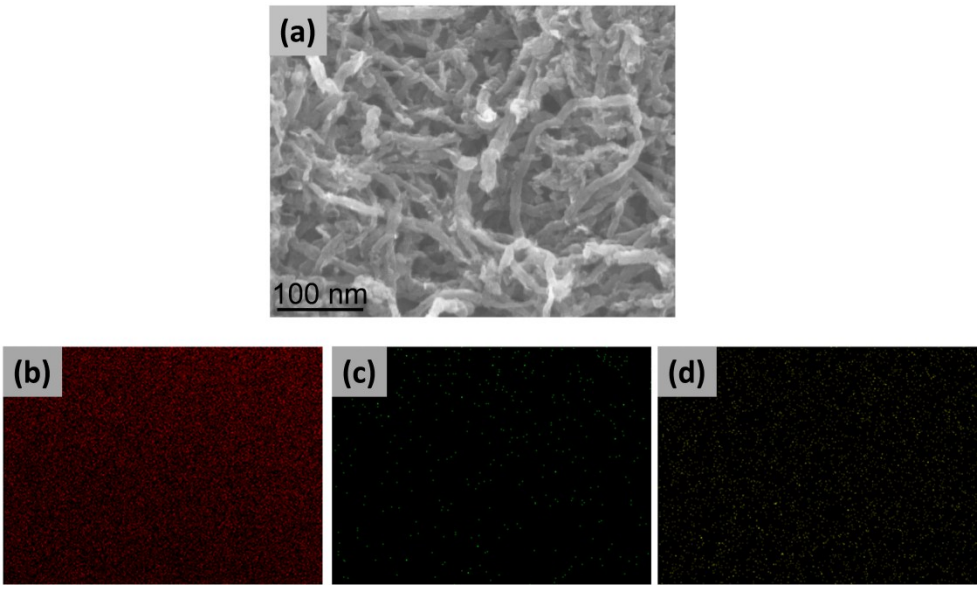

Fig. S3 SEM image (a), and EDS maps: C map (b), O map (c), and Mn map (d) of the as-synthesized Mn^{2+}-OCNT.

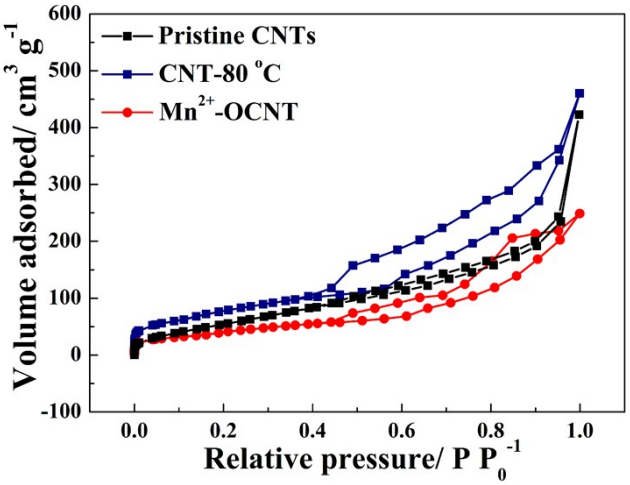

Fig. S4 Nitrogen adsorption-desorption isotherms of samples.

Table S1 Textural properties of different samples.

Catalysts	SSAs (m^2 g^{-1})	Average pore diameter (nm)	Pore volume (cm^3 g^{-1})
Pristine CNTs	210.0	11.2	0.59
CNT-80°C	284.1	10.0	0.71
Mn^{2+}-OCNT	153.6	10.0	0.38

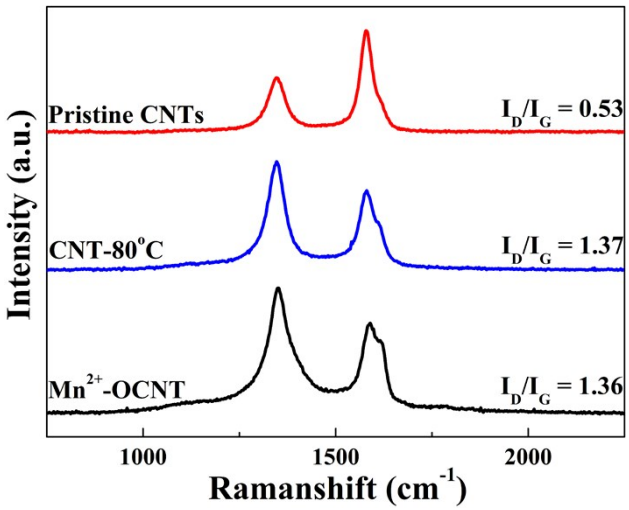

Fig. S5 Raman spectra of samples.

Table S2 The element composition of Mn^{2+}-OCNT and Mn^{2+}-CNT_{HNO_3} detected by XPS measurement.

Samples	C (at%)	O (at%)	Mn (at%)
Mn^{2+}-OCNT	86.01	12.64	1.35
Mn^{2+}-CNT_{HNO_3}	97.55	2.32	0.13

Table S3 Mn content in various samples (ICP results).

Samples	Mn^{2+}-OCNT	Mn^{2+}-CNT_{HNO_3}	1st-used Mn^{2+}-OCNT	2nd-used Mn^{2+}-OCNT	3rd-used Mn^{2+}-OCNT	Alkali-treated Mn^{2+}-OCNT
Mn content (wt%)	1.85	0.04	1.63	1.48	1.38	1.83

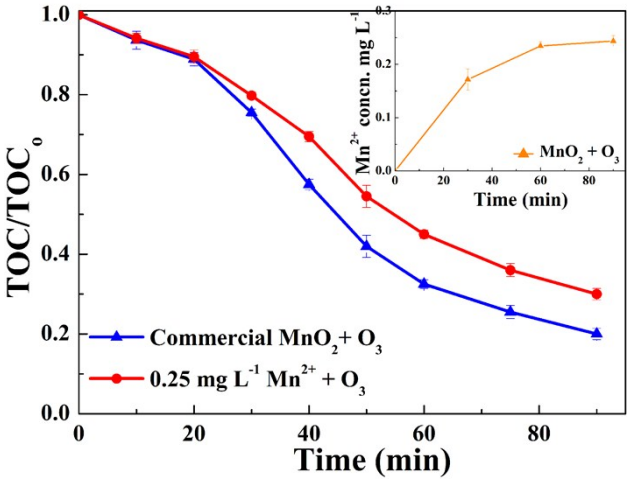

Fig. S6 Mineralization efficiencies of phenol in different reaction systems, and Mn^{2+} concentration in solution as a function of time in MnO_2/O_3 system (the inset in Fig. S6) (Experimental conditions: [phenol] = 20 mg L^{-1}, [O_3] = 10 mg L^{-1}, initial pH 6.2).

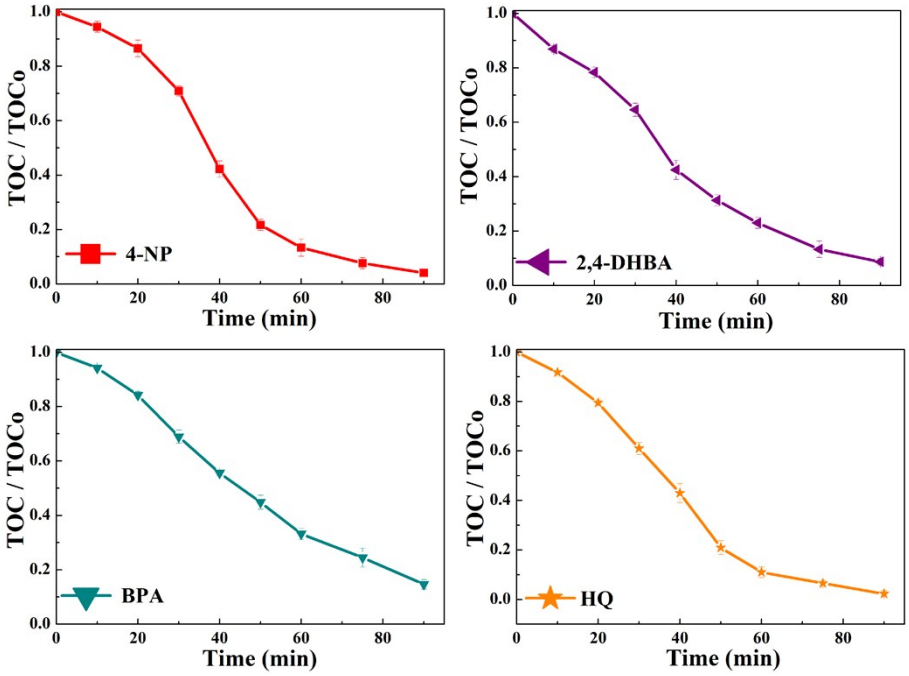

Fig. S7 Mineralization efficiencies of different phenol compounds in Mn^{2+}-OCNT/O_3 system (Experimental conditions: [pollutant] = 20 mg L^{-1}, [Mn^{2+}-OCNT] = 0.028 g L^{-1}, [O_3] = 10 mg L^{-1}).

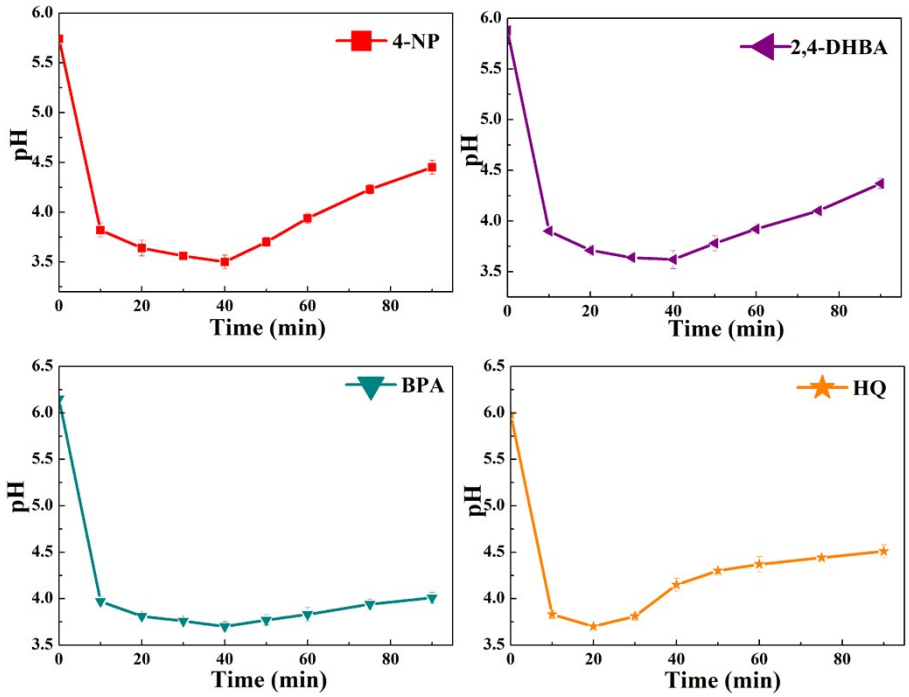

Fig. S8 Variations of solution pH during different pollutants degradation in Mn^{2+}-OCNT/O_3 system (Experimental conditions: [pollutant] = 20 mg L^{-1}, [Mn^{2+}-OCNT] = 0.028 g L^{-1}, [O_3] = 10 mg L^{-1}).

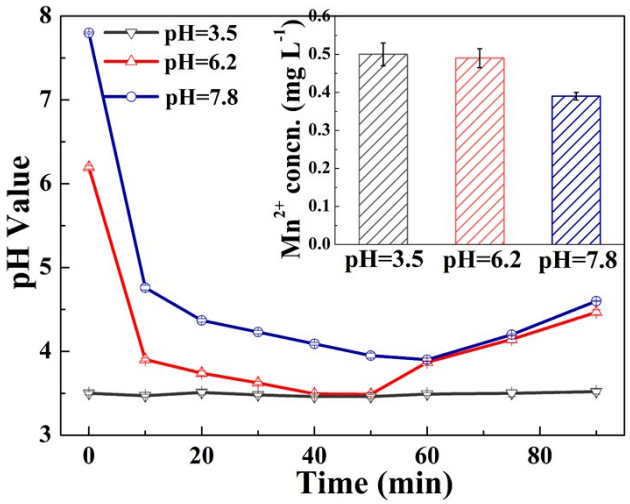

Fig. S9 Variations of solution pH and the maximum Mn^{2+} concentration (the inset in Fig. S9) in the Mn^{2+}-OCNT/O_3 system under different initial solution pH (Experimental conditions: [phenol] = 20 mg L^{-1}, [catalyst] = 0.028 g L^{-1}, [O_3] = 10 mg L^{-1}).

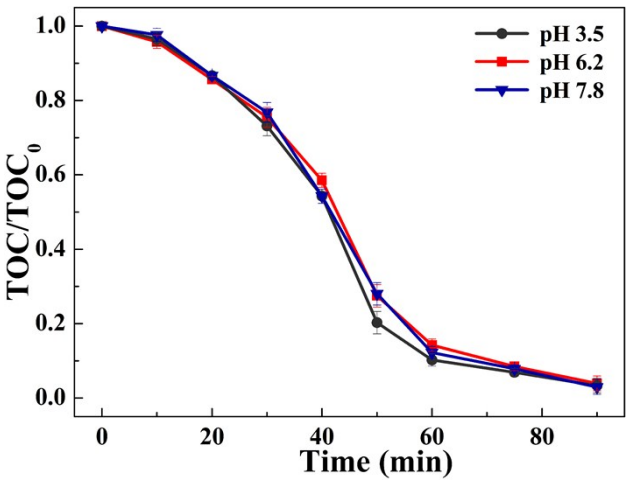

Fig. S10. Effect of solution pH on phenol mineralization in homogeneous Mn^{2+}/O_3 system (Experimental conditions: [phenol] = 20 mg L^{-1}, [Mn^{2+}] = 0.52 mg L^{-1}, [O_3] = 10 mg L^{-1}).

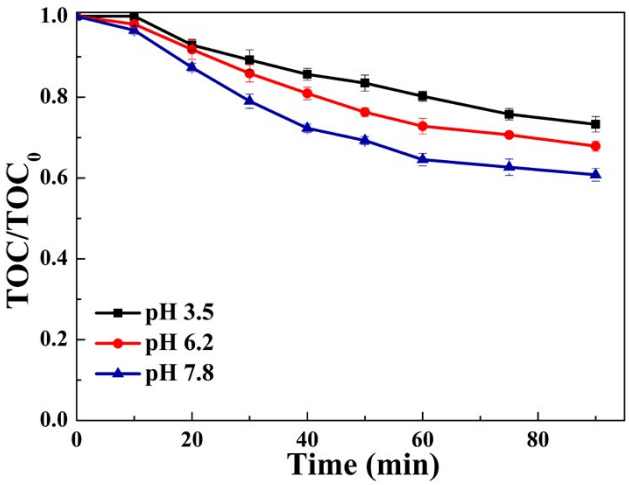

Fig. S11 Effect of solution pH on mineralization efficiency of phenol in ozonation alone ([phenol] = 20 mg L^{-1}, [O_3] = 10 mg L^{-1}).

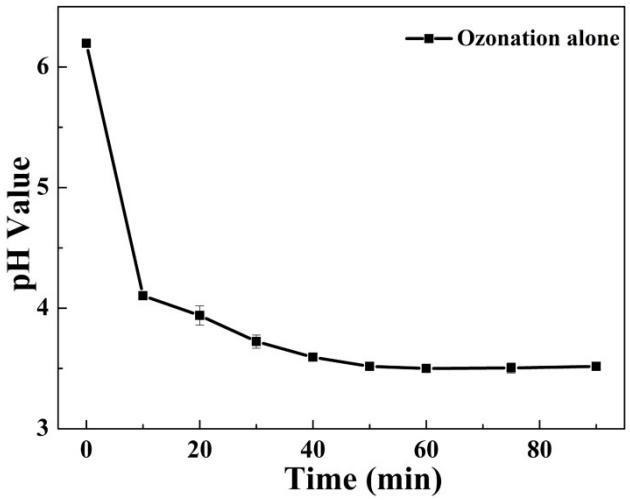

Fig. S12 Variations of solution pH during phenol degradation in ozonation alone (Experimental conditions: [phenol] = 20 mg L^{-1}, [O_3] = 10 mg L^{-1}, initial pH 6.2).

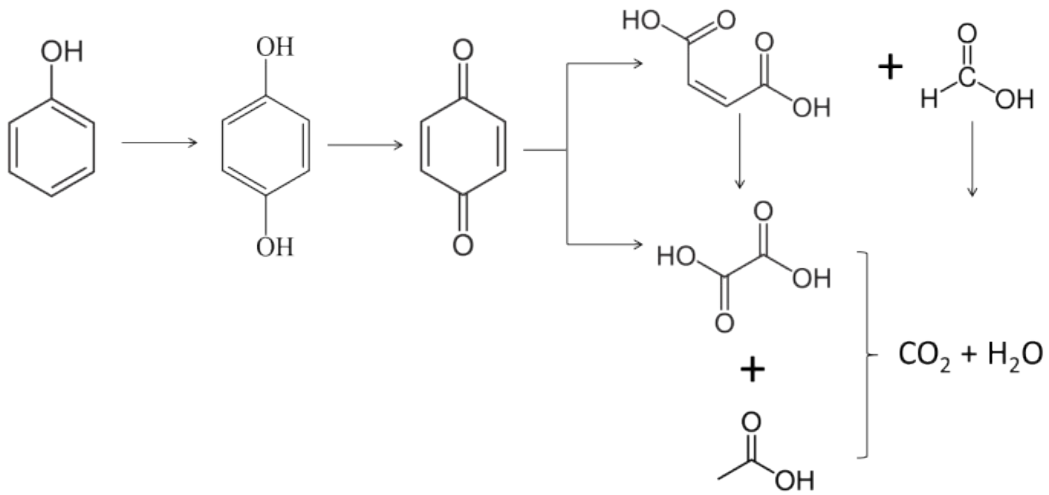

Fig. S13 Reaction pathway of phenol during catalytic ozonation.

Table S4 Main intermediates of phenol degradation.

Retention time (min)	Product	Molecular structure
9.549	hydroquinone	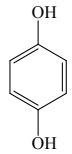
6.695	p-benzoquinone	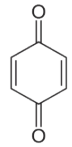
7.07	formic acid	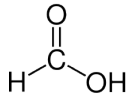
7.37	acetic acid	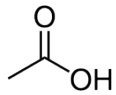
7.60	oxalic acid	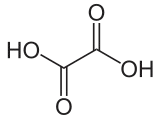
8.77	maleic acid	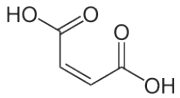

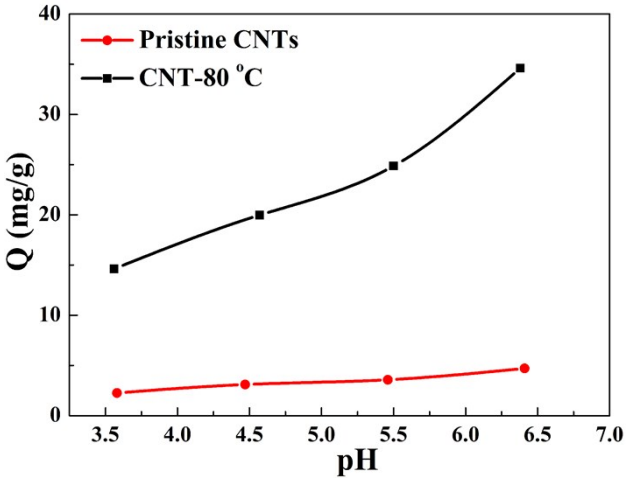

Fig. S14 Adsorption capacity of Mn^{2+} on pristine CNTs and CNT-80 °C (Experimental conditions: [initial Mn^{2+}] = 10 mg L^{-1}, m/V = 0.1 g/L, *T* = room temperature, solution pH was adjusted by 0.01 M NaOH or $HClO_4$).

To investigate the Mn adsorption capacity on different CNT samples, batch adsorption experiments were carried out under pH 3.5-6.6 and in 0.001-0.1 M $NaClO_4$

solutions. The solution pH was adjusted by 0.01 M NaOH or $HClO_4$. The suspensions of Mn^{2+} and CNTs were shaken for 2 h to achieve the sorption equilibrium. The adsorption capacity (Q, mg/g) of Mn^{2+} on CNT surfaces as a function of solution pH was shown in Fig. S14. Under various experimental conditions investigated, the adsorption capacities for Mn^{2+} on OCNT are much higher than those on CNT_{HNO_3}. Notably, the adsorption capacity of Mn^{2+} on OCNT surfaces is mainly dependent on solution pH. The adsorption capacity slowly increases when the solution pH is increased, and achieves the maximum with 37.6 mg g^{-1} Mn^{2+} adsorbed at pH of 6.4.

Table S5 Mechanism of homogeneous catalytic ozonation by Mn^{2+}.

$Mn^{2+} + O_3 + H^+ \rightarrow Mn^{3+} + \bullet OH + O_2$	(1)
$2Mn^{3+} + 2H_2O \rightarrow Mn^{2+} + MnO_2 + 4H^+$	(2)
$MnO_2 + Inter. + 4H^+ \rightarrow Mn^{2+} + CO_2 + H_2O$	(3)
$2MnO_2 + O_3 + 6H^+ \rightarrow 2Mn^{7+} + 2O_2 + 3H_2O$	(4)
$Mn^{7+} + Org. + H_2O \rightarrow MnO_2 + H^+ + Inter.$	(5)

During the homogeneous Mn^{2+}/O_3 process, the dissolved Mn^{2+} reacts with O_3 to form •OH, which effectively mineralizes organic pollutants. At the same time, Mn^{2+} is oxidized into Mn^{3+} (Eq. (1)), which possess extremely poor stability in water and can be easily transferred into Mn^{2+} and Mn^{4+} (Eq. (2)). The Mn^{4+} could oxidize the organic intermediates into CO_2 and H_2O with the simultaneous regeneration of Mn^{2+} (Eq. (3)). Alternatively, the generated Mn^{4+} could be oxidized into Mn^{7+} by O_3 (Eq. (4)) when the pollutant concentrations became low. Mn^{7+} is a strong oxidant (E^o (MnO_4^-, $8H^+/Mn^{2+}$) = 1.51 V vs NHE), which can easily capture the organic intermediates (Eq. (5)). However, compared with homogeneous Mn^{2+}/O_3 system, the concentration of Mn^{7+} during the Mn^{2+}-OCNT/O_3 system is much lower (as shown in Fig. S15). This indicates little Mn^{7+} was generated or the generated Mn^{7+} could be consumed immediately during the Mn^{2+}-OCNT/O_3 system. With the degradation of organics, solution pH elevated to induce the adsorption of dissolved Mn^{2+}, which

could hinder the oxidation of Mn^{2+} into Mn^{7+}. Moreover, the generated Mn^{7+} can react with C, forming MnO_2 on OCNT surfaces.[2]

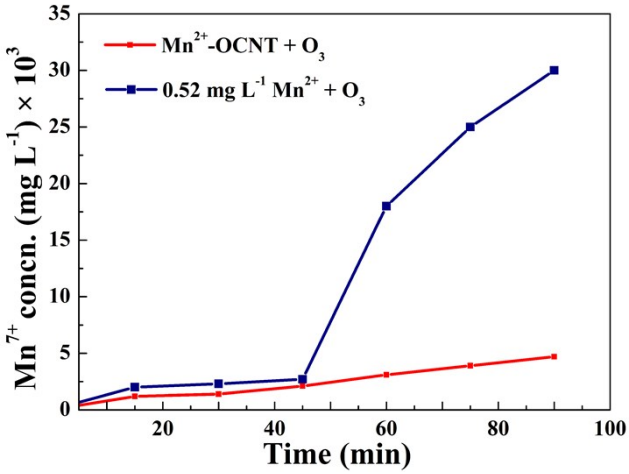

Fig. S15 The Mn^{7+} concentration as a function of time during Mn^{2+}-OCNT/O_3 and homogeneous Mn^{2+}/O_3 systems.

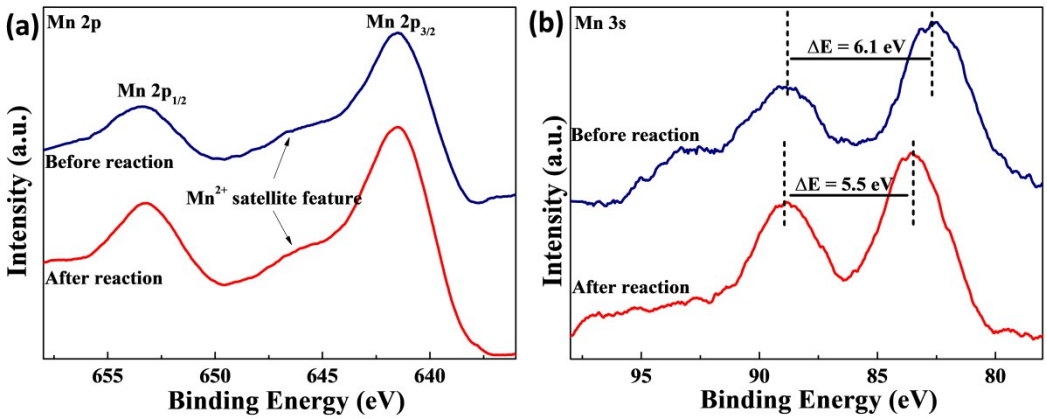

Fig. S16 Mn 2p (a) and Mn 3s (b) regions of the XPS spectra for the Mn^{2+}-OCNT samples before and after the reaction.

To verify the change of Mn chemical state in the Mn^{2+}-OCNT/O_3 system, XPS spectra of Mn^{2+}-OCNT before and after reactions were recorded. The Mn 2p spectra (Fig. S16a) of catalysts before and after reactions both show two characteristic peaks at around 653.4 and 641.5 eV, which correspond to the Mn $2p_{1/2}$ and Mn $2p_{3/2}$ spin–orbit components of manganese oxides (MnO_x) respectively.[3,4] The binding energies of Mn $2p_{1/2}$ and Mn $2p_{3/2}$ for MnOx generally lie within a narrow range, thus causing difficulty in the identification of Mn valence state by the sole Mn 2p spectrum.[3,5]

However, the spectra also exhibit a satellite feature at ~646 eV which is only presented for Mn^{2+}.[6] This result reveals the existence of Mn^{2+} on both fresh and used Mn^{2+}-OCNT. Notably, it has been reported that the magnitude of peak splitting (ΔE) of Mn 3s peak can be used as a diagnostic characteristic of Mn valence state.[5,7] Therefore, Mn 3s regions of Mn^{2+}-OCNT before and after reactions were also collected to attain a straightforward identification of the Mn valence state. By deconvolution of Mn 3s from XPS spectra, the average oxidation state (AOS) of Mn could be determined by the following equation:[8]

$$AOS = 8.95 - 1.13\Delta E \qquad (1\text{-}6)$$

Where ΔE represents the energy difference between the two main peaks.

Fig. S16b shows two multiple-split components, which result from the coupling of non-ionized 3s electron with 3d valence-band electrons. The ΔE value for the fresh Mn^{2+}-OCNT is 6.1 eV, which corresponded to an AOS value of 2.06. This result revealed the valence state of Mn on the as-synthesized Mn^{2+}-OCNT was Mn^{2+}. After reaction, the ΔE value slightly reduces to 5.5 eV, corresponding to an AOS of 2.7. This suggests a small portion of Mn^{2+} is converted into a relatively high valence state. The Mn^{2+} can be converted into Mn^{4+} and Mn^{7+} when the solution pH is increased. The generated Mn^{7+} can react with C, forming MnO_2 on OCNT surfaces.[2] Consequently, the slight reduction of the ΔE value in the Mn 3s spectrum could be attributed to the generation of Mn^{4+} on Mn^{2+}-OCNT surfaces.

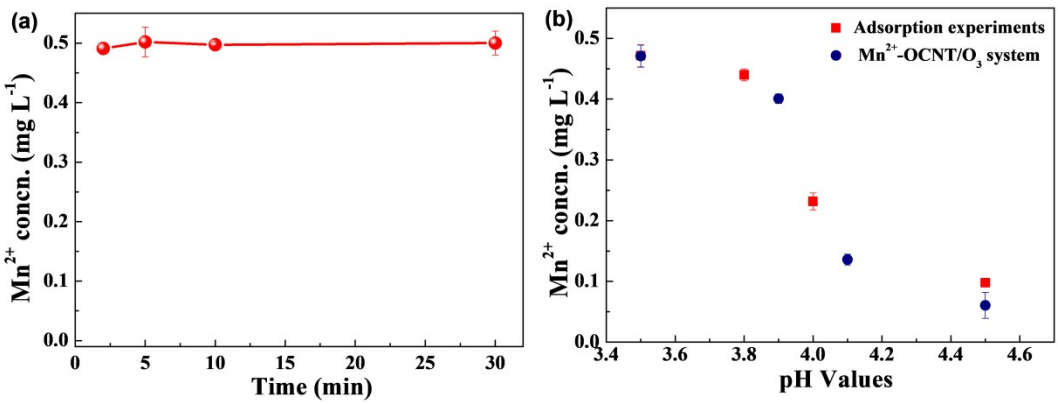

Fig. S17 Desorption amounts of Mn^{2+} as a function of desorption time at pH 3.5 in the Mn^{2+}-OCNT suspension (a); Comparisons of desorbed Mn^{2+} concentrations during the Mn^{2+}-OCNT/O_3

system and Mn^{2+} adsorption experiment as a function of solution pH (b).

To estimate the contribution of each process to the recovery of desorbed Mn^{2+} during the Mn^{2+}-OCNT/O_3 system, batch Mn^{2+} adsorption experiments were examined in Mn^{2+}-OCNT suspension (without the presence of O_3). The pH of the Mn^{2+}-OCNT suspension was first adjusted to 3.5 by 0.1 M HCl solution. After the suspension was stirred for 30 min to achieve the Mn^{2+} desorption equilibrium, Mn^{2+} adsorption experiments were carried out under pH 3.5-4.5. Fig. S17a shows the desorption equilibrium is established as < 2.5 min under pH 3.5, which means Mn^{2+} can rapidly desorb from the Mn^{2+}-OCNT surfaces. Notably, the desorption amounts of Mn^{2+} at pH 3.5 (0.47 mg L^{-1}) is nearly identical to that of Mn^{2+}-OCNT/O_3 system after 50 min of reaction (pH ~3.5, 0.48 mg L^{-1}). This further reveals that the dissolved Mn^{2+} in the solution is a result of the desorption of Mn^{2+} caused by the decreased solution pH during the Mn^{2+}-OCNT/O_3 system. For the Mn^{2+} adsorption experiments, Fig. S17b shows when the suspension pH increases from 3.5 to 4.5, the Mn^{2+} concentration in the solution is gradually decreased. The recovery ratio of desorbed Mn^{2+} at pH value of 3.8, 4.0, and 4.5 is 15%, 56%, and 81%, respectively. Because the solubility product constant (Ksp) of $Mn(OH)_2(s)$ is ~2×10^{-13}, Mn^{2+} begins to form precipitation at pH~10.2 with the largest Mn^{2+} concentration of 0.52 mg L^{-1}. This means Mn mainly exists in the form of ionic Mn in the solution under pH range between 3.5 and 4.5. Therefore, it can be concluded that the recovery of Mn^{2+} is attributed to the re-adsorption of Mn^{2+} during the Mn^{2+} adsorption experiment. Fig. S17b also shows that the desorbed Mn^{2+} concentrations for Mn^{2+} adsorption experiments demonstrate similar changes as the result of Mn^{2+}-OCNT/O_3 system under pH 3.5-4.5. However, although at the same pH of 4.5, the Mn^{2+} recovery ratio for the Mn^{2+}-OCNT/O_3 system at 90 min is 88%, slightly higher than 81% for the Mn^{2+} adsorption experiment. The contribution of re-adsorption process to Mn^{2+} recovery is ~92% in the Mn^{2+}-OCNT/O_3 system at 90 min.

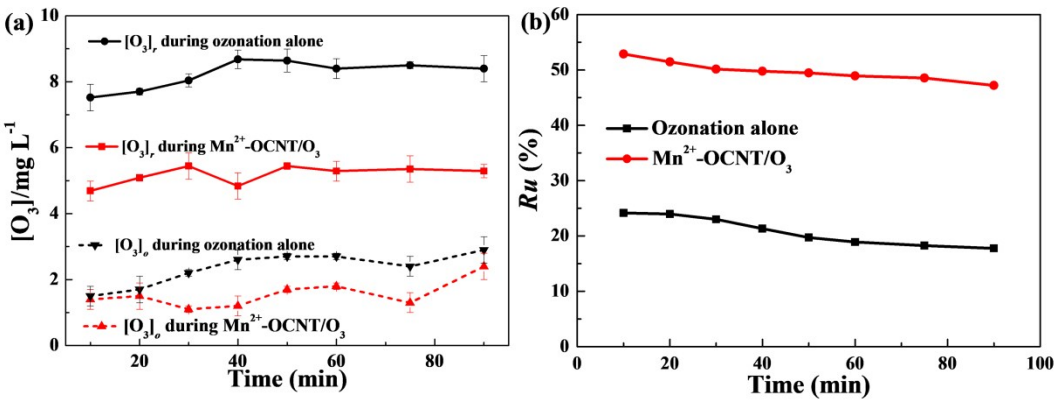

Fig. S18 Residual ozone $[O_3]_r$ and off gas O_3 concentration $[O_3]_o$ (a) and the utilization efficiency of O_3 (b) as a function of time in different processes.

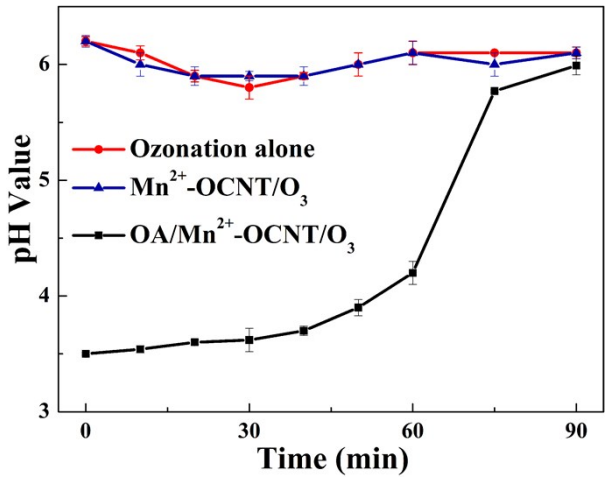

Fig. S19 Variations of solution pH in different reaction systems (Experimental conditions: [phenol] = 20 mg L^{-1}, [Mn^{2+}-OCNT] = 0.028 g L^{-1} (if used), $[O_3]$ = 10 mg L^{-1}, initial pH 6.2 (except OA/Mn^{2+}-OCNT/O_3 system)).

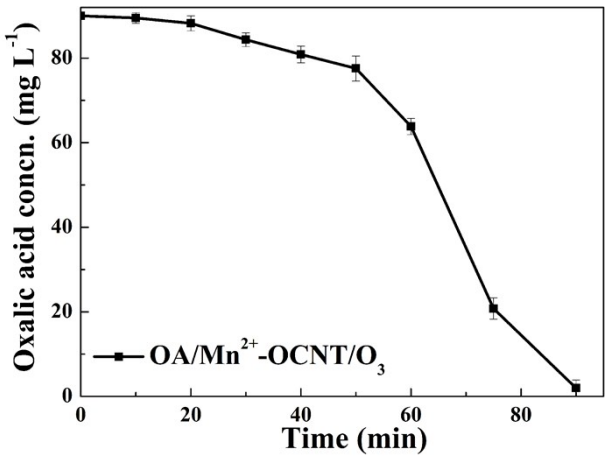

Fig. S20 The change of oxalic acid concentration during OA/Mn^{2+}-OCNT/O_3 system (Experimental conditions: [phenol] = 20 mg L^{-1}, [Mn^{2+}-OCNT] = 0.028 g L^{-1}, $[O_3]$ = 10 mg L^{-1}).

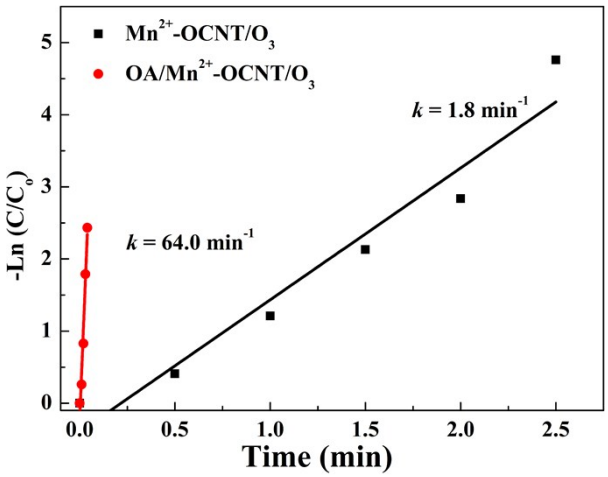

Fig. S21 Kinetics of phenol degradation in different reaction systems (Experimental conditions: [phenol] = 500 μg L^{-1}, [Mn^{2+}-OCNT] = 0.028 g L^{-1}, [O_3] = 10 mg L^{-1}).

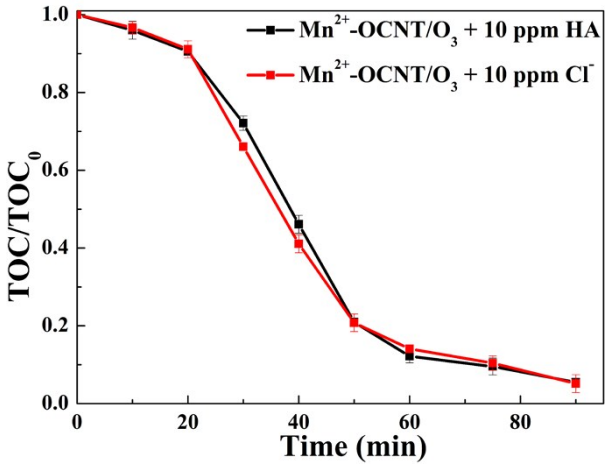

Fig. S22 Mineralization efficiencies of phenol in different reaction systems (Experimental conditions: [phenol] = 20 mg L^{-1}, [Mn^{2+}-OCNT] = 0.028 g L^{-1}, [O_3] = 10 mg L^{-1}, initial pH 6.2)

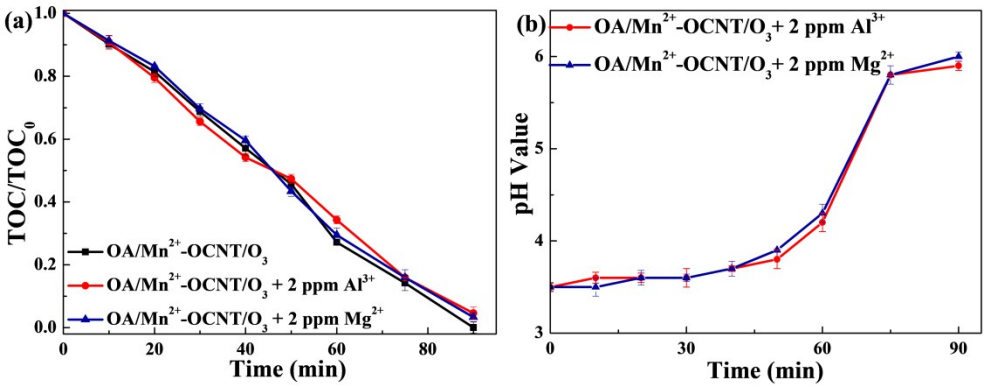

Fig. S23 Mineralization efficiencies of phenol in different reaction systems (a); Variations of solution pH in different reaction systems (b) (Experimental conditions: [phenol] = 20 mg L^{-1}, [Mn^{2+}-OCNT] = 0.028 g L^{-1}, [O_3] = 10 mg L^{-1}, initial pH 6.2 buffered with 3 mM $NaOH/KH_2PO_4$).

Table S6 The parameters of the wastewater quality.

COD	TOC	conductivity	pH
91.2 mg L^{-1}	33.6 mg L^{-1}	2.0 ms cm^{-1}	7.8

Table S7 The metal ions in the wastewater.

ion species	Concentration (mg L^{-1})
Na^{+}	1030.4
K^{+}	540.0
Mg^{2+}	27.0
Zn^{2+}	/
Ca^{2+}	90.4
Mn^{2+}	0.09
$Fe^{(2+,\ 3+)}$	0.004
$Cu^{(1+,\ 2+)}$	/
Al^{3+}	/
Total Cd	0.002
Total Cr	/

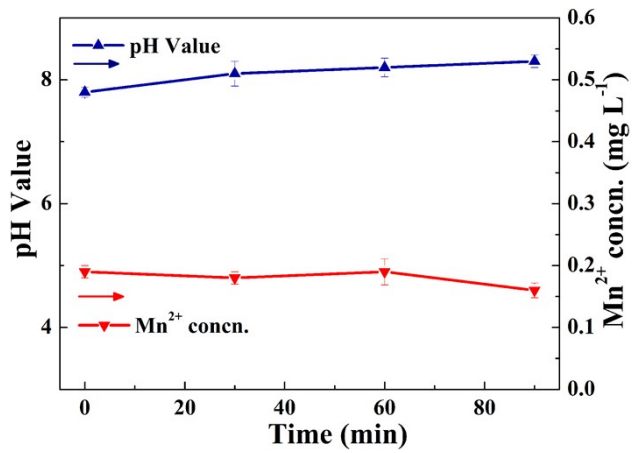

Fig. S24 Variations of solution pH and dissolved Mn^{2+} concentration as a function of time during the Mn^{2+}-OCNT/O_3 system (Experimental conditions: [Mn^{2+}-OCNT] = 0.028 g L^{-1}, [O_3] = 10 mg L^{-1}).

REFERENCE

(1) Li, X. Y.; Cui, Y. H.; Feng, Y. J.; Xie, Z. M.; Gu, J. D. Reaction pathways and mechanisms of the electrochemical degradation of phenol on different electrodes. *Water Res*., **2005**, 39 (10), 1972-1981.

(2) Gan, Z. X.; Xiong, S. J.; Wu, X. L.; He, C. Y.; Shen, J. C.; Chu, P. K. Mn2+-bonded reduced graphene oxide with strong radiative recombination in broad visible range caused by resonant energy transfer. Nano lett. 2011, 11 (9), 3951-3956.

(3) Tan, B. J.; Klabunde, K. J.; Sherwood, P. M. XPS studies of solvated metal atom dispersed (SMAD) catalysts. Evidence for layered cobalt-manganese particles on alumina and silica. *J. Am. Chem. Soc*. **1991**, 113 (3), 855-861.

(4) Lei, Z.; Zhang, J.; Zhao, X. S. Ultrathin MnO_2 nanofibers grown on graphitic carbon spheres as high-performance asymmetric supercapacitor electrodes. *J. Mater. Chem*. **2012**, 22 (1), 153-160.

(5) Thermo scientific XPS. https://xpssimplified.com/elements/manganese.php.

(6) Wang, J.; Chen, S.; Quan, X.; Yu, H. T. Fluorine-doped carbon nanotubes as an efficient metal-free catalyst for destruction of organic pollutants in catalytic ozonation. *Chemosphere* **2018**, 190, 135-143

(7) Toupin, M.; Brousse, T.; Bélanger, D. Influence of microstucture on the charge storage properties of chemically synthesized manganese dioxide. *Chem. Mater.* **2002**, 14 (9), 3946-3952.

(8) Andreozzi, R.; Caprio, V.; Marotta, R.; Tufano, V. Kinetic modeling of pyruvic acid ozonation in aqueous solutions catalyzed by Mn (II) and Mn (IV) ions. *Water Res*. **2001**. 35 (1), 109-120.